Decomposing the Atmospheric Flow Using Potential Vorticity Framework

EERO HOLOPAINEN AND JUSSI KAUROLA

Department of Meteorology, University of Helsinki, Helsinki, Finland

(Manuscript received 20 September 1990, in final form 14 June 1991)

ABSTRACT

The invertibility principle of potential vorticity (PV) is used, within a quasigeostrophic framework, to formally partition the observed atmospheric flow in various ways. The first method separates the contributions of the interior PV and temperature at the lower boundary. In the literature, this approach has mainly been applied to some idealized flows. In real situations, however, this partitioning appears questionable because any nonzero temperature anomaly at the boundary automatically implies a nonzero stability part of the interior PV and, hence, these two contributions never occur independent of each other in nature. At large horizontal scales, the two contributions have a large amplitude at every level and almost cancel each other. The second method decomposes the 3D flow into contributions arising from the vorticity and the stability parts of the PV. This formal partitioning appears essentially to decompose the flow into its barotropic and baroclinic part. The third method explores the role of PV of various layers in inducing the flow. This approach shows that the upper-level flow is very little influenced by PV at the lower levels. In the lower troposphere, however, the large-scale flow is dictated by PV in the upper troposphere and lower stratosphere, whereas the smaller-scale features are induced by the local PV, the latter including the effect of the boundary temperature. The third method may be useful as means of verification of atmospheric general circulation models.

1. Introduction

Potential vorticity (PV) is the backbone of dynamic meteorology. If the distribution of PV in the fluid interior and the distribution of temperature at the boundaries are known, the fields of temperature, pressure, and wind can be obtained by an "inversion." Hoskins et al. (1985) give a thorough discussion of the history of the PV concept and the invertibility principle and illustrate them with some simple examples. An example of inverting the PV distribution in the case of a shallow-water free-surface model has been worked out by McIntyre and Norton (1990) and Egger (1990). Robinson (1988) used the inversion of PV to investigate how flows in the middle atmosphere are determined. As far as the authors know, the invertibility principle has not been used to study real tropospheric 3D flows.

In this paper we study tropospheric flows using the invertibility principle of quasigeostrophic PV in isobaric coordinates. The theoretical basis is explained in section 2. In section 3 we discuss the numerical methods and data used, and test the numerical inversion algorithm. The remaining sections present various methods of decomposing the flow.

The first method, discussed by Hoskins et al. (1985), deals with the flow contributions arising from the interior PV and temperature anomalies at the boundaries. It is shown that a separate treatment of the interior and boundary contributions, though mathematically correct, gives questionable results. The second method decomposes the flow into contributions arising from the vorticity and the stability parts of PV. It appears that the flow is essentially decomposed into barotropic and baroclinic components. The third method enables one to explore the role of PV of various layers in inducing the flow. This approach has been used by Robinson (1988). As discussed in section 6, the third method used here might have applications in the verification of atmospheric general circulation models.

2. Theoretical framework

a. The quasigeostrophic inversion problem

The discussion of the present paper is to a large extent heuristic. It is based on the concept of quasigeostrophic potential vorticity q, defined in pressure coordinate system as

$$q = f + \frac{1}{f_o}\nabla_p^2\Phi'' + f_o\frac{\partial}{\partial p}\left(\frac{1}{\sigma_{\text{ref}}}\frac{\partial\Phi''}{\partial p}\right),$$

where Φ'' is geopotential anomaly (in this paper "anomaly" refers to a deviation from an isobaric average), f the Coriolis parameter (f_o = const = 10^{-4} s^{-1}), $\sigma = -\alpha/\theta(\partial\theta/\partial p)$ is the static stability, α being the specific volume and θ the potential tem-

Corresponding author address: Dr. Eero Holopainen, Department of Meteorology, University of Helsinki, Hallituskatu 11-13, SF-00100 Helsinki, Finland.

perature, ∇_p is the horizontal gradient operator at a pressure surface, and σ_{ref} is the "reference" static stability, function of pressure only.

Symbolically, the expression for $q - f$ can be written as

$$L(\Phi'') = \text{VORT} + \text{STAB}, \tag{1}$$

where

$$L(\ \ ) = \frac{1}{f_o}\nabla_p{}^2 + f_o\frac{\partial}{\partial p}\left(\frac{1}{\sigma_{\text{ref}}}\frac{\partial}{\partial p}\right),$$

and

$$\text{VORT} = \frac{1}{f_o}\nabla_p{}^2\Phi'' \tag{2}$$

$$\text{STAB} = f_o\frac{\partial}{\partial p}\left(\frac{1}{\sigma_{\text{ref}}}\frac{\partial\Phi''}{\partial p}\right) \tag{3a}$$

$$= f_o\frac{\partial}{\partial p}\left(\frac{\theta''}{d\theta_{\text{ref}}/dp}\right). \tag{3b}$$

The boundary conditions (BC) are

$$\left(\frac{\partial\Phi''}{\partial p}\right)^{\text{vort}} = 0, \quad \text{at} \quad p = 0 \quad \text{and} \quad p = p_o \tag{4a}$$

$$\left(\frac{\partial\Phi''}{\partial p}\right)^{\text{stab}} = \begin{cases} 0, & \text{at} \quad p = 0 \\ -\alpha'', & \text{at} \quad p = p_o, \end{cases} \tag{4b}$$

where p_o is the pressure at the lowest level used (here 1000 mb).

Since the rhs of (1) and (4b) can be inferred from observations, the 3D distribution of Φ'' can be solved. The temperature and horizontal and vertical velocity fields can be obtained by applying the hydrostatic and geostrophic relationships and the "omega" equation, respectively. Thus, the entire flow pattern can be constructed, if one knows the PV in the fluid interior together with the temperature at the lower boundary. The problem of calculating Φ'' from (1) and (4) is a simple example of application of the general invertibility principle discussed by Hoskins et al. (1985).

Inversion of the system (1) and (4) makes it possible to partition the total flow in several alternative ways. The traditional approach is to write

$$\Phi'' = \Phi''(\text{PV}) + \Phi''(\text{BC}), \tag{5}$$

where $\Phi''(\text{PV})$ is the part arising from the 3D distribution of PV in the interior with homogeneous boundary conditions, and $\Phi''(\text{BC})$ is the part arising from the temperature distribution at the boundary with PV = 0 in the interior.

A second, purely formal, way of partitioning the flow is to write

$$\Phi'' = \Phi''(\text{VORT}) + \Phi''(\text{STAB, BC}), \tag{6}$$

where $\Phi''(\text{VORT})$ is the contribution arising from the VORT and $\Phi''(\text{STAB, BC})$ from the STAB part of the PV (BC stands for the nonzero boundary condition for the STAB part).

A third way of decomposing the flow into component fields is obtained by dividing the whole atmosphere into k layers. The anomalous geopotential field is then obtained by writing

$$\Phi'' = \sum_k \Phi_k'', \tag{7}$$

where Φ_k'' denotes the contribution of Φ'' arising from the PV in the kth layer.

b. *Analytic examples*

Equation (1) can be solved analytically for simple "source functions" VORT and STAB if static stability is held constant (σ_o). In this case (1) takes the form:

$$\left(\frac{1}{f_o}\nabla^2 + \frac{f_o}{\sigma_o}\frac{\partial^2}{\partial p^2}\right)\Phi'' = \text{VORT} + \text{STAB}. \tag{8}$$

In the following examples, we shall study the inversion of (8) separately for the VORT and STAB part of the PV.

Let STAB = 0 and VORT be given by the expression

$$\text{VORT} = \text{Re}\{Be^{i(kx+ly)}\},$$

where k and l are the wavenumbers in the x and y direction, respectively, and B is a constant. Assuming a solution of the form

$$\Phi'' = \text{Re}\{A(p)e^{i(kx+ly)}\},$$

the solution to (8) with boundary condition (4a) is:

$$\Phi'' = \text{Re}\left\{-\frac{B}{\mu^2}e^{i(kx+ly)}\right\}, \tag{9}$$

where $\mu^2 = (k^2 + l^2)/f_o{}^2$. Positive (negative) VORT thus induces a low (high) geopotential anomaly.

In the second example, it is assumed that VORT = 0 and

$$\frac{\theta''}{d\theta_{\text{ref}}/dp} = -Q(x, y)\left(\frac{p - p_t}{p_o - p_t}\right),$$

where p_t and p_o denote the pressure at the top and bottom of the atmosphere, and $Q(x, y)$ gives the horizontal pattern. In this case

$$\text{STAB} = f_o\frac{\partial}{\partial p}\left(\frac{\theta''}{d\theta_{\text{ref}}/dp}\right) = -f_o\frac{Q(x, y)}{p_o - p_t},$$

and the boundary conditions, corresponding to (4b), are

$$\left(\frac{\partial\Phi''}{\partial p}\right)^{\text{stab}} = \begin{cases} 0, & \text{at} \quad p = p_t \\ -\sigma_o Q(x, y), & \text{at} \quad p = p_o. \end{cases} \tag{10}$$

If $Q(x, y)$ is wavelike:

$$Q(x, y) = \mathrm{Re}\{Q_o e^{i(kx+ly)}\},$$

where Q_o is a constant, the solution to (8) satisfying the boundary condition (10) is

$$\Phi'' = \mathrm{Re}\left\{\frac{\sigma_o Q_o}{\Delta p}\left[\frac{1}{\mu^2} - \frac{\Delta p}{\mu}\frac{e^{\mu(p_t-p)} + e^{-\mu(p_t-p)}}{e^{\mu\Delta p} - e^{-\mu\Delta p}}\right]e^{i(kx+ly)}\right\}, \quad (11)$$

I II

where $\Delta p = p_o - p_t$. Formally, the term I is due to the STAB term with homogeneous boundary conditions, term II due to the boundary condition with STAB = 0. This analytic solution was first discussed by Lau and Holopainen (1984) (see their Fig. 1).

In the limit of $\mu \to 0$, term I approaches $+\infty$ and term II $-\infty$, while their sum remains finite. Hence, in the case of long waves, the contributions of BC and STAB cancel each other to a large extent.

3. Numerical methods and the data used

At each pressure level, the fields were expanded in terms of spherical harmonics

$$\Phi'' = \sum_{n,m} \chi_n^m(p) Y_n^m \quad (12a)$$

$$G = \sum_{n,m} C_n^m(p) Y_n^m, \quad (12b)$$

where G stands for VORT or STAB, n is the total, m the zonal wavenumber, and Y the spherical harmonic function; χ and C are pressure-dependent coefficients. For each component n, m (1) can be written in the form:

$$\left\{-\frac{n(n+1)}{f_o a^2} + \frac{f_o}{\sigma_{\mathrm{ref}}}\frac{\partial^2}{\partial p^2} - \frac{f_o}{\sigma_{\mathrm{ref}}^2}\frac{\partial \sigma_{\mathrm{ref}}}{\partial p}\frac{\partial}{\partial p}\right\}\chi_n^m = C_n^m, \quad (13)$$

where a is the radius of the earth. The boundary condition (4) gives

$$\left(\frac{\partial \chi_n^m}{\partial p}\right)^{\mathrm{vort}} = 0, \quad \text{when} \quad p = p_o, p_t \quad (14a)$$

$$\left(\frac{\partial \chi_n^m}{\partial p}\right)^{\mathrm{stab}} = -B_n^m, \quad \text{when} \quad p = p_o, p_t, \quad (14b)$$

where B is determined by the distribution of the boundary temperature and p_t is the highest level used (here 10 mb). All quantities (C, B, and σ_{ref}) were interpolated by using cubic splines into a vertical grid with a grid interval of 10 mb, and (13) was solved using the band matrix method (for further details see the Appendix). The expansion (12) was truncated at ($n = 30$, $m = 20$). The numerical scheme was tested in the case of the analytical solution (11) discussed earlier.

Figure 1 shows a zonal cross section of v_g and θ induced by a hypothetical temperature anomaly with a wavy structure ($n = 15$, $m = 8$) in the horizontal, and an amplitude decaying linearly from 5 K at 1000 mb to zero at the top of the atmosphere. Because of a realistically varying σ_{ref} (calculated from the data for February 1979 for the region 30°–90°N), the response can only be obtained numerically. However, the results are qualitatively similar to the analytic solution (11) obtained with a constant static stability.

In agreement with the findings by Hoskins (1983) and Hoskins et al. (1985), Fig. 1a shows that a warm (cold) anomaly at the lower boundary induces cyclonic (anticyclonic) circulation in the atmosphere above. However, the interior PV (the STAB term) induces a wind pattern (Fig. 1b) almost opposite to that induced by the mere boundary temperature anomaly (Fig. 1a). Their sum (Fig. 1c) shows a cyclonic circulation in the lower troposphere and an anticyclonic circulation in the upper troposphere above the warm anomaly, with a reversed distribution above the cold anomaly. The degree of counterbalancing between v_g(BC) and v_g(STAB) in Fig. 1 is indicated by the maxima of v_g at 1000 mb; these are 16.0 m s^{-1}, 10.4 m s^{-1}, and 5.6 m s^{-1} in panels a, b, and c, respectively.

Though VORT was set equal to zero in the "forcing," Fig. 1c, for example, shows that in the response vorticity is clearly not zero. It could be thought that this vorticity is generated by an instantaneous adjustment process, which is needed for the response to satisfy the hydrostatic and geostrophic relationships. In this geostrophic adjustment process, the fraction of PV that is converted from STAB to VORT depends primarily on the horizontal scale of the wave.

A flow pattern qualitatively similar to that seen in Fig. 1c occurs in the real atmosphere in the Northern Hemisphere in summer, when the air is relatively warm over land masses and cold over the oceans and when, on the average, one observes a "thermal low" in the low troposphere over the continents and a "thermal high" over the oceans (see, e.g., Fig. 1 in Holopainen 1970).

When applying the inversion algorithm to the real atmosphere, the so-called First GARP Global Experiment (FGGE) "final" analyses from the European Centre for Medium Range Weather Forecasts for 19 pressure levels from 10 mb to 1000 mb were used to calculate the rhs of (1) and (4b), while σ_{ref} was taken to be the average global stability in February 1979. Calculations were performed for several synoptic cases, but only the results for the Northern Hemisphere at 0000 UTC 21 February 1979 will be discussed here. The fields obtained by inverting (1) and (4) with the rhs calculated from the original analyses will be called the "reconstructed analyses."

Before studying the performance of the inversion

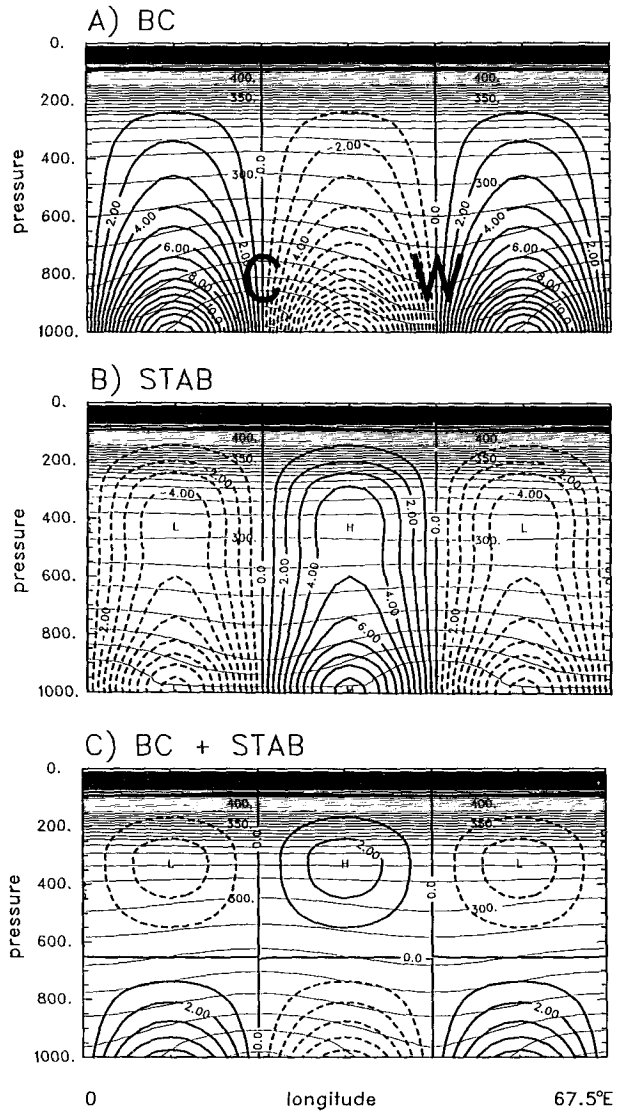

FIG. 1. Zonal cross section (from 0° to 67.5°E along 52°N) of geostrophic meridional wind component v_g (heavy lines every 1 m s^{-1}, dashed lines indicate negative values), induced by a hypothetical temperature anomaly that has a (n = 15, m = 8) wave structure in the horizontal. The amplitude is 5 K at 1000 mb, decaying linearly with the pressure to zero at 10 mb. Letters W and C in panel (a) indicate the location of the imposed warm and cold anomaly. The thin lines are isentropes (reference state + perturbation) every 5 K. The contribution into v_g and θ are shown from (a) the boundary temperature with STAB = 0 in the interior and (b) STAB determined with homogeneous boundary conditions; (c) is the sum of (a) and (b).

algorithm, it is useful to look at the components of the PV distribution at some levels. Figure 2 shows the patterns of VORT and STAB at the 300- and 850-mb levels. At 300 mb the VORT field proves to be more dominated by much smaller horizontal scales than the STAB field. The latter is characterized by large positive values in the high latitudes. At 850 mb the magnitudes of both the VORT and the STAB fields are typically smaller than those at 300 mb.

Figure 3 compares the original and reconstructed $Z'' = \Phi''/g_o$ (g_o = 9.807 m s^{-2}) anomalies at 500 and 1000 mb. The inversion algorithm is found to perform properly. The small differences are caused by the STAB term being calculated directly from the potential temperature analyses using expression (3b). Numerical solution also produces some smoothing.

4. Contributions from the interior PV and the boundary temperature

Figure 4 shows the partitioning of the 500-mb height anomaly into contributions arising from the interior PV and from the boundary temperature. The patterns are qualitatively the same for all pressure levels. Here Z''(BC) is essentially due to the temperature anomaly at 1000 mb: the results (not shown) obtained with the 10-mb temperature anomaly set equal to zero cannot be distinguished from those in Fig. 4b. The sum of the fields in Figs. 4a and 4b is seen in Fig. 3b. An almost total counterbalancing between Z''(PV) and Z''(BC) is evident.

As discussed in connection with Fig. 1, a cold temperature anomaly at the lower boundary formally induces an anticyclonic circulation into the air column above. The large-scale temperature anomaly at 1000 mb is always dominated by negative anomalies in the polar regions and positive anomalies at lower latitudes. Therefore, it is not surprising that Z''(BC) shows (Fig. 4b) an anticyclone at the pole. The maximum value of Z'' near the pole is 14 741 m.

In the map of Z''(PV) (Fig. 4a), we find a polar depression. This is due to the fact that at high latitudes the STAB term is positive and large (of the order of f), particularly in the upper troposphere (see Fig. 2b). In the inversion algorithm, which gives the largest amplitudes for small wavenumbers (see section 2b), this STAB distribution results in a Z''(PV) pattern with an axisymmetric structure and a very large amplitude: the minimum near the pole is −15 520 m and the speed of the implied westerly wind in midlatitudes is more than 200 m s^{-1}. The large-scale counterbalancing between the contributions by the boundary temperature and the STAB term was anticipated by Hoskins et al. (1987) in their response to the comment by Green (1987) on the original paper by Hoskins et al. (1985).

If the small wavenumber contributions are excluded from the STAB and BC terms, more realistic amplitudes are obtained for Z''(PV) and Z''(BC). For example, when the contributions from waves with $n \leq 6$ are excluded, the amplitude of both Z''(PV) and Z''(BC) are of the order of a few hundred meters. However, a relatively large compensation between the two fields (not shown) is still a dominant feature. Long waves are also to a large extent filtered out if one studies day-to-day changes in the height field. However, coun-

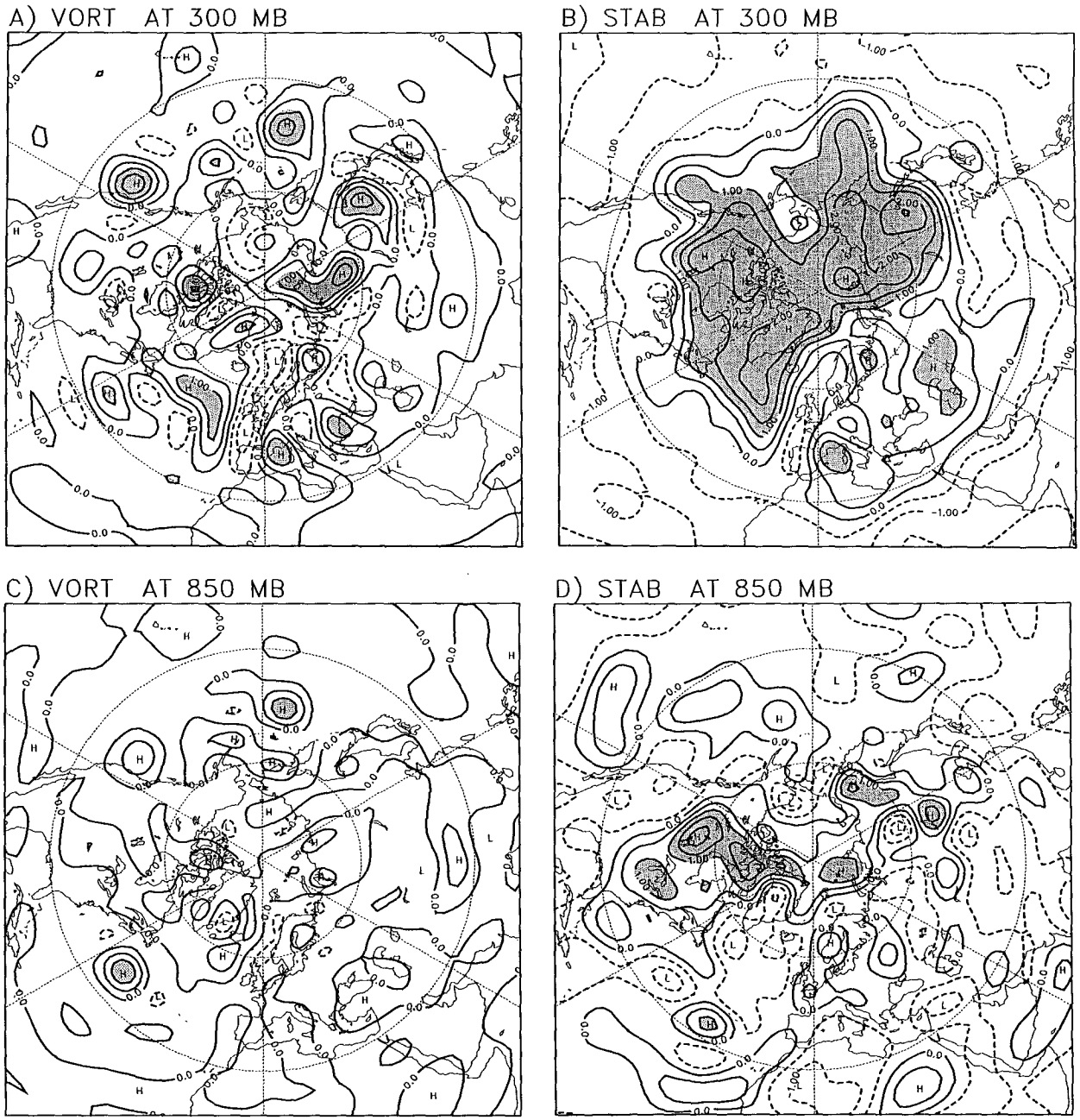

FIG. 2. VORT and STAB [for expressions, see (2)–(3)] at 300 and 850 mb at 0000 UTC 21 February 1979. Isoline spacing is 0.5×10^{-4} s^{-1}. Negative values are indicated by dashed contours, and areas with values larger than 1×10^{-4} s^{-1} are shaded.

terbalancing between the contributions of the boundary temperature and interior PV is still evident.

Thus, it appears that partitioning of the flow according to (5), even if mathematically correct, is questionable. In a way this is not surprising, because any nonzero temperature anomaly at the boundary automatically implies a nonzero STAB term. Hence, a discussion of STAB and BC viewed separately from each other is not physically relevant. This finding is further supported by the fact that fields almost identical to those shown in Figs. 3b and 3d were obtained by setting θ'' equal to zero at the top and the bottom of the atmosphere; that is, homogeneous boundary conditions were used and the STAB term was calculated with $\theta'' = 0$ at the boundaries. This method is the numerical counterpart of the use of Dirac delta function discussed by Bretherton (1966), and has already been discussed by Lau and Holopainen (1984).

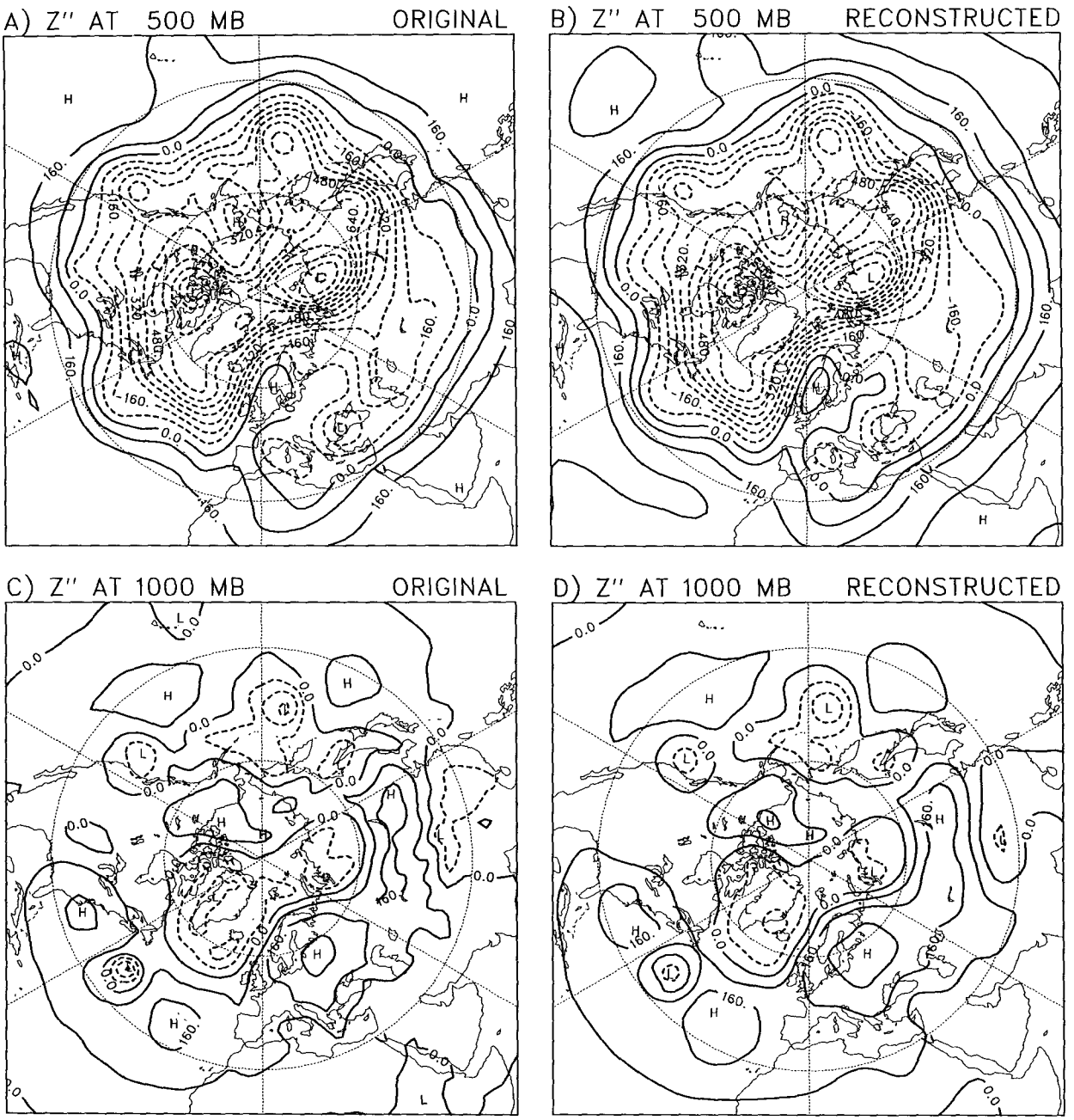

FIG. 3. Original analyses of the isobaric height field Z'' at 0000 UTC 21 February 1979 at (a) 500 mb and (c) 1000 mb. Reconstructed analyses (see text) at (b) 500 mb and (d) 1000 mb. Isoline spacing is 80 m; negative values are indicated by dashed lines.

5. Contributions from the vorticity and stability part of potential vorticity with their respective boundary conditions

Figure 5 shows the contributions to the 300- and 1000-mb Z'' fields by the vorticity and stability part of PV. The fields of Z''(VORT) are seen to have almost the same pattern in the upper and lower troposphere, whereas the pattern of Z''(STAB, BC) at 300 mb is almost negative to that at 1000 mb. The vertical integral of Z''(STAB, BC) is zero and, consequently, the 500-mb Z''(STAB, BC) (not shown) nearly vanishes. On the basis of Fig. 5 it is clear that Z''(VORT) in the atmosphere is connected essentially with barotropic structures and Z''(STAB, BC) with baroclinic structures.

Decomposing of the flow into contributions induced by VORT and STAB is purely formal (and is, in fact,

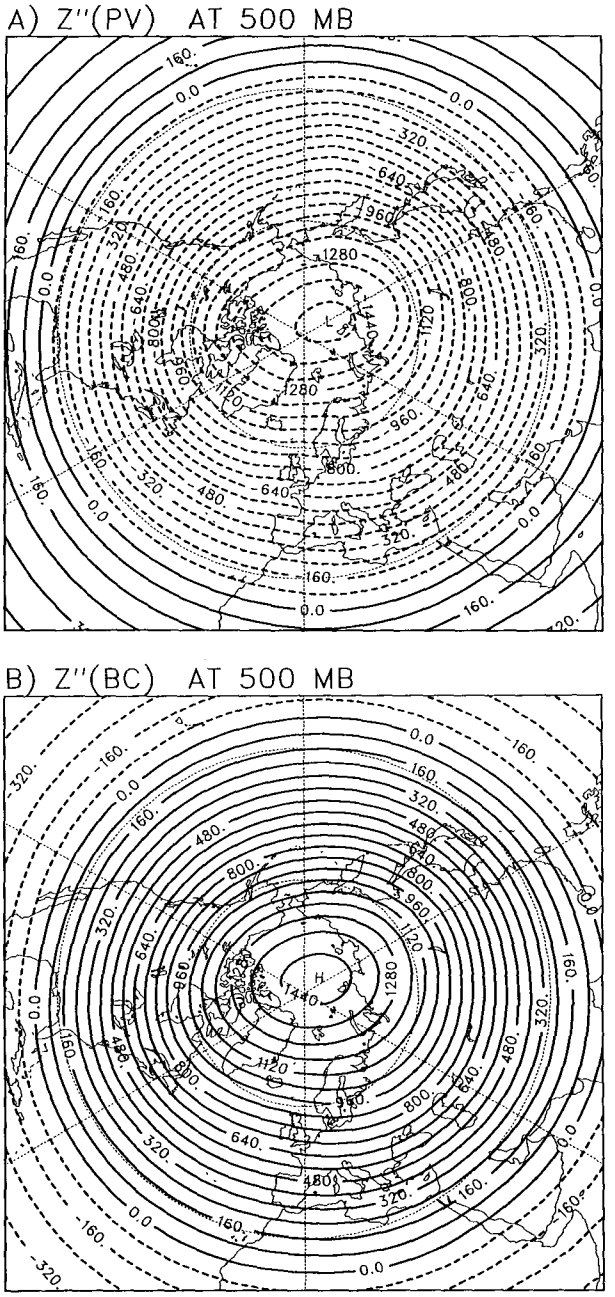

FIG. 4. Decomposing the Z'' field at 0000 UTC 21 February 1979 at 500 mb into contributions from the interior PV (a) and the boundary temperature (b). Minimum value in (a) is −15 520 m, maximum value in (b) 14 741 m; isoline spacing is 800 m. Note that the sum of (a) and (b) is that shown in Fig. 3b.

not possible in the case of Ertel's potential vorticity). It defeats the purpose of PV analysis because, in adiabatic frictionless flow, VORT + STAB (but not VORT and STAB individually) is conserved following the geostrophic flow. Nevertheless, it is of interest to note that the method of decomposing the flow into barotropic and baroclinic components, as first done by Wiin-Nielsen (1962) and Smagorinsky (1963) and later, for example, by Tanaka (1985), appears to arise as a consequence of the quasigeostrophic PV framework.

6. Contributions from the potential vorticity in various layers

This section studies how effective the PV in various layers is in inducing the flow. This problem was dealt with by Robinson (1988) for the stratosphere and mesosphere.

The numerical algorithm for determining decomposition (7) sets

$$\text{VORT} = 0 \quad \text{and} \quad \theta'' = 0$$

outside the kth layer, and applies nonzero boundary condition at the top and/or the bottom of the atmosphere only if the layer k is adjacent to one of these boundaries (for details see the Appendix). In this manner the atmosphere could be divided into layers, the sum contribution of which gives exactly, without any assumptions, the total reconstructed geopotential field. In the temperature anomaly fields, there are jumps from zero to the observed values at the lower boundary of the layer and back to zero at the upper boundary. In addition to VORT and STAB, the total PV within the layer k thus includes a thin PV "sheet" (cf. Bretherton 1966) just below the layer and another sheet, with opposite sign, just above the layer. The PV sheets at the boundary of two adjacent layers cancel each other.

Before looking at the results obtained with observed PV and BC distributions it is useful to consider some simple cases. Let us arbitrarily assume that, in a layer k, the horizontal fields of VORT and STAB are wavelike with a constant amplitude of 1×10^{-4} s^{-1}. In the case of the STAB part, the amplitude of the temperature anomaly is then proportional to $pd\theta_{\text{ref}}/dp$; positive STAB anomaly implies a negative temperature anomaly in the layer k.

Figure 6 shows the response (Z'') to these arbitrary PV sources by the inversion algorithm. The response to a PV source in the form of VORT is seen to be entirely different from that to STAB: while the former has the same sign at all levels, the latter has a dipole character in the vertical direction. The PV sheets discussed above are crucial for the character of the response seen in Figs. 6b and 6d. If the layer considered is made smaller, the amplitude of the height response is correspondingly reduced and becomes more peaked than those seen in Fig. 6.

Figure 6 shows that a PV source in the stable environment of the upper layer causes a stronger local response than a similar source in the lower troposphere. However, the vertical penetration of the response is, in the case of low troposphere PV, much larger than

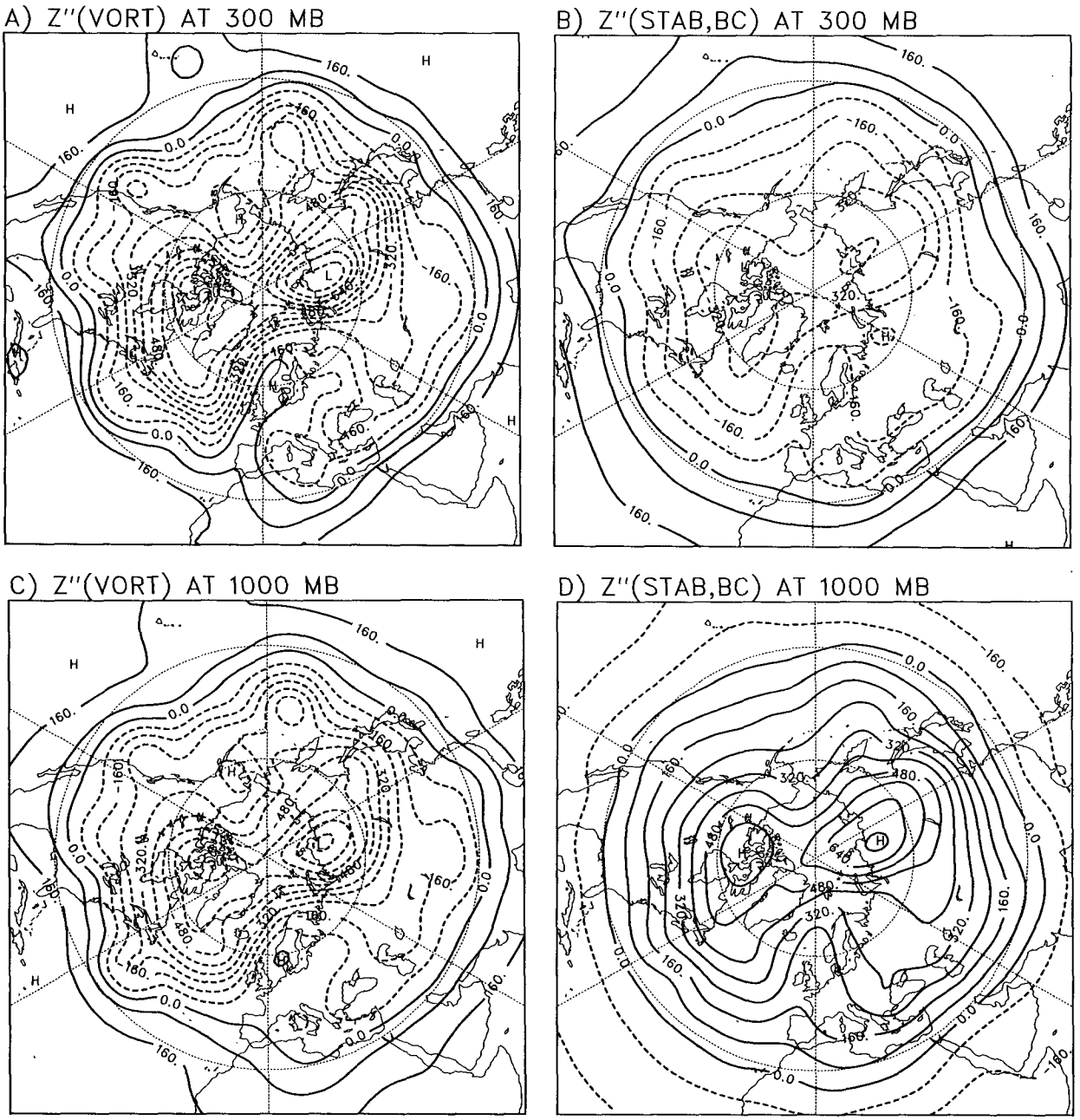

FIG. 5. Decomposing the Z'' field at 0000 UTC 21 February 1979 at 300 mb (upper panels) and at 1000 mb (lower panels) into contributions arising from the VORT term (panels a and c), and from the STAB term with the associated boundary temperatures (panels b and d). Note that the sum of (c) and (d) is that shown in Fig. 3d. Isoline spacing is 80 m, negative values are indicated by dashed lines.

in the case of the upper-level PV. These features are due to the vertical distribution of the σ_{ref}, as reported by Robinson (1988) and Pfeffer (1987).

Concerning the wavenumber dependence of the response, the results in Fig. 6 show that an upper-level VORT source on long waves is capable of inducing flow also in the lower troposphere; this feature (which is very weak on short waves) has been earlier pointed out, for example, by Robinson (1988).

Figure 7 shows the contributions to the 1000-mb Z'' field by observed PV in various layers. Most of the small-scale features at 1000 mb are induced by the PV in the lower atmosphere (Fig. 7d). The layers above 500 mb induce a westerly flow at 1000 mb. This upper-level contribution occurs at very large horizontal scales, in agreement with the discussion of Fig. 6. The westerly flow associated with the upper troposphere PV, however, is to a large extent counterbalanced by the con-

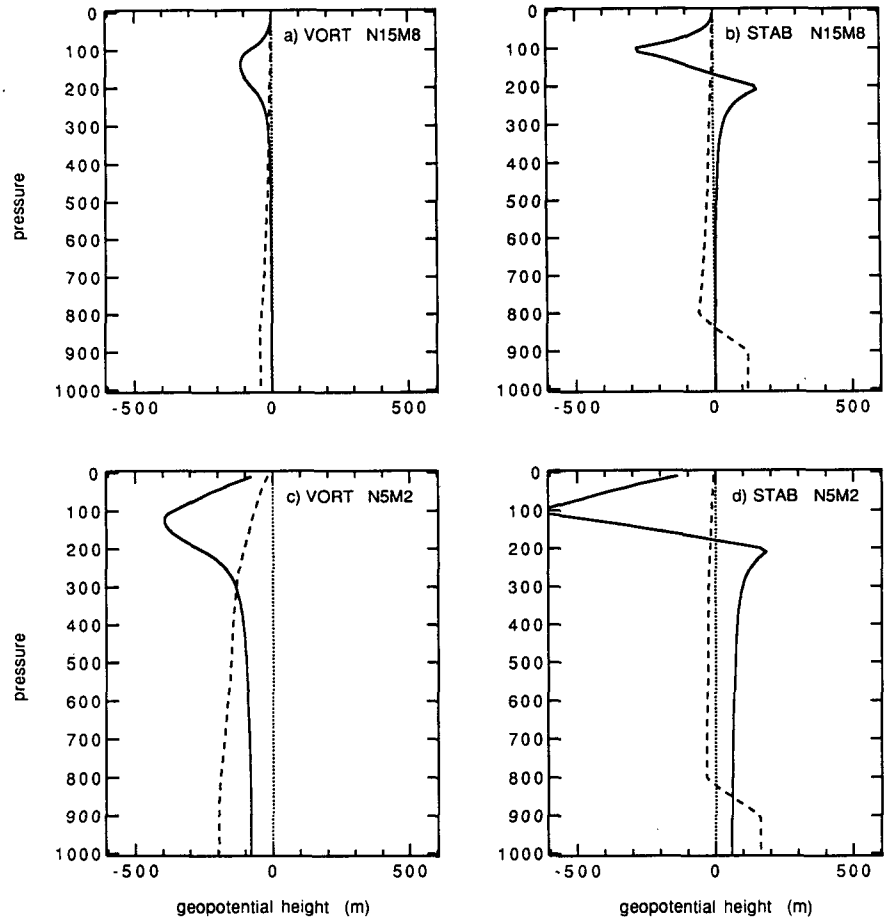

FIG. 6. The influence of constant PV (1×10^{-4} s^{-1}) in a specified 100-mb layer on the amplitude of the Z'' wave. PV is located in the layer 100–200 mb (continuous curve), and in the 800–900-mb layer (dashed curve). The upper panels refer to the ($n = 15$, $m = 8$) wave, the lower panels to the ($n = 5$, $m = 2$) wave. In the lhs panels the PV is in the form of VORT, in the rhs panels in the form of STAB.

tributions of the lower troposphere: in panels 7c and 7d there is, in addition to the small-scale features mentioned above, an anticyclone over the polar latitudes. This can be understood in light of the fact that, in the lower troposphere, Z''_k(VORT) is smaller than Z''_k(STAB, BC) (maps not shown), and the positive stability anomalies prevailing at high latitudes induce at 1000 mb an anticyclone at the pole. This is in accordance with the dashed curves in Figs. 6b and 6d.

Figure 8 shows the contributions to the 500-mb Z'' field arising from PV in various layers. Comparison of the panels shows the similarity of the flow patterns induced by the PV in, on the one hand, all layers above 500 mb and, on the other hand, all layers below 500 mb. The contribution of the upper layers proved to be dominated by the VORT part of the PV, whereas both the STAB and VORT terms are important for the contribution of the lower layers. The flow patterns induced by the layers in the immediate vicinity of the 500-mb level (Figs. 8b and 8c) are likewise very similar to each other. The flow induced by the PV of the lowest layer (1000–850 mb) (Fig. 8d) is negligible, whereas the PV of the uppermost layer (200–10 mb) (Fig. 8a) induces a moderate large-scale westerly circulation.

The almost nil contribution of the lowest layer (Fig. 8d) contrasts with the huge anticyclone induced by the 1000-mb temperature when treated separately (see Fig. 4b). Accordingly, if a partitioning of the tropospheric flow on the basis of the PV framework is to be at all meaningful, method (7) might be preferable to method (5).

7. Summary and discussion

Our paper demonstrates that it is possible in real situations to invert the PV and obtain a good facsimile of the original total flow. This is not surprising, however, because we have first used this very same flow to estimate the quasigeostrophic PV, and then simply inverted the associated three-dimensional operator. [We

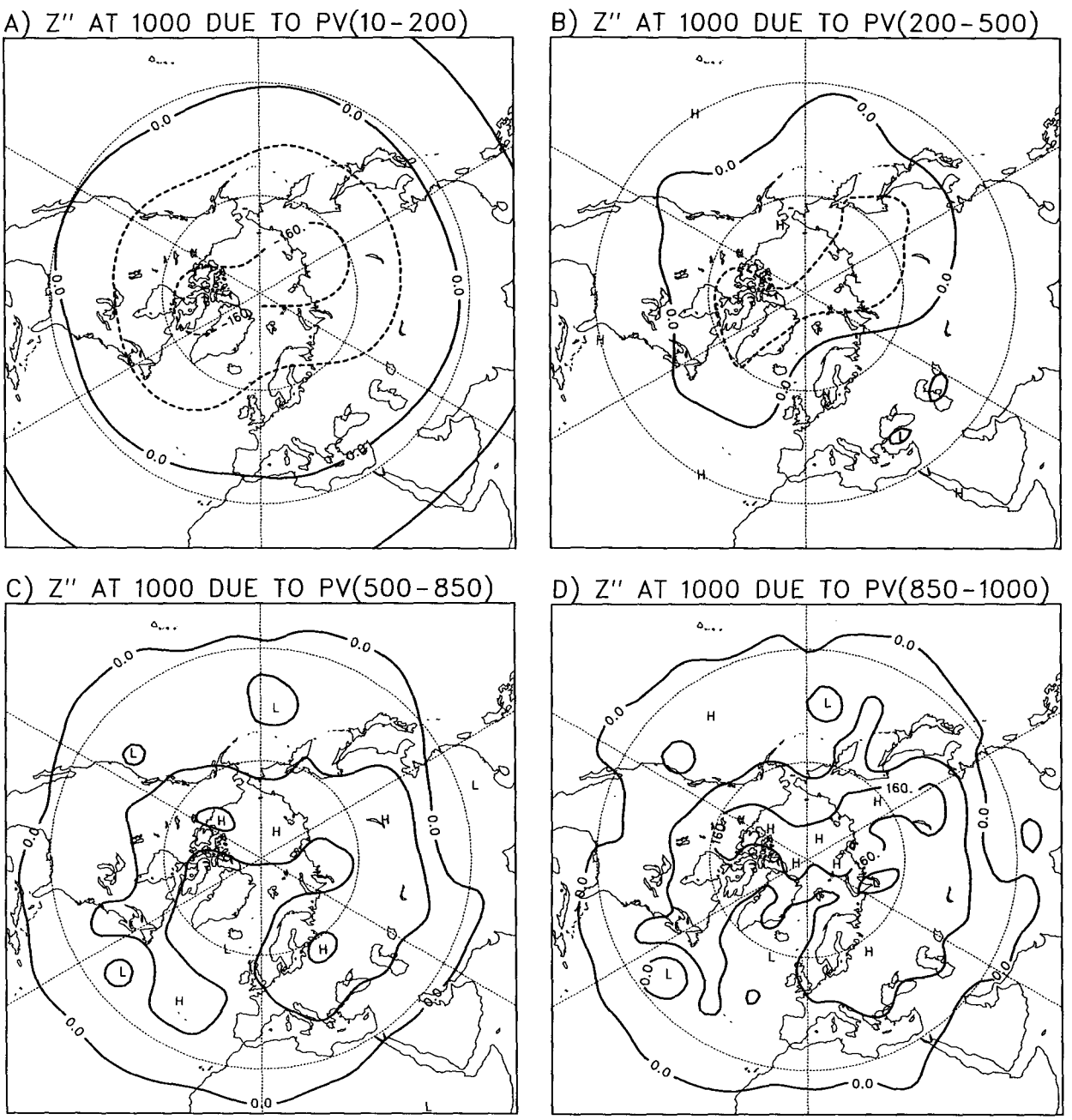

FIG. 7. Contributions to the 1000-mb Z'' field at 0000 UTC 21 February 1979 arising from the PV in the layers indicated. The sum of the four fields is that seen in Fig. 3d. Note that (d) includes the contribution by the 1000-mb temperature, and (a) the small contribution by the 10-mb temperature. Isoline spacing is 80 m, negative values are indicated by dashed lines.

have not discussed here the validity of the quasigeostrophic system for the dynamics of the atmospheric large-scale flow; such a discussion is found, e.g., in Hoskins (1983) and Hoskins et al. (1985)].

We have demonstrated that problems of interpretation arise as soon as one starts making decompositions of the flow. For example, according to traditional thinking, atmospheric flow consists of contributions of the interior PV and the boundary temperature. This kind of decomposition, even if mathematically correct, appears questionable because any nonzero temperature anomaly at the boundary automatically implies a nonzero STAB term for the interior and, hence, these two contributions never occur independent of each other in nature. (This reservation concerns only the inversion products; of course, a fundamental aspect of PV is that it is a tracer, as is also the boundary temperature in idealized cases.)

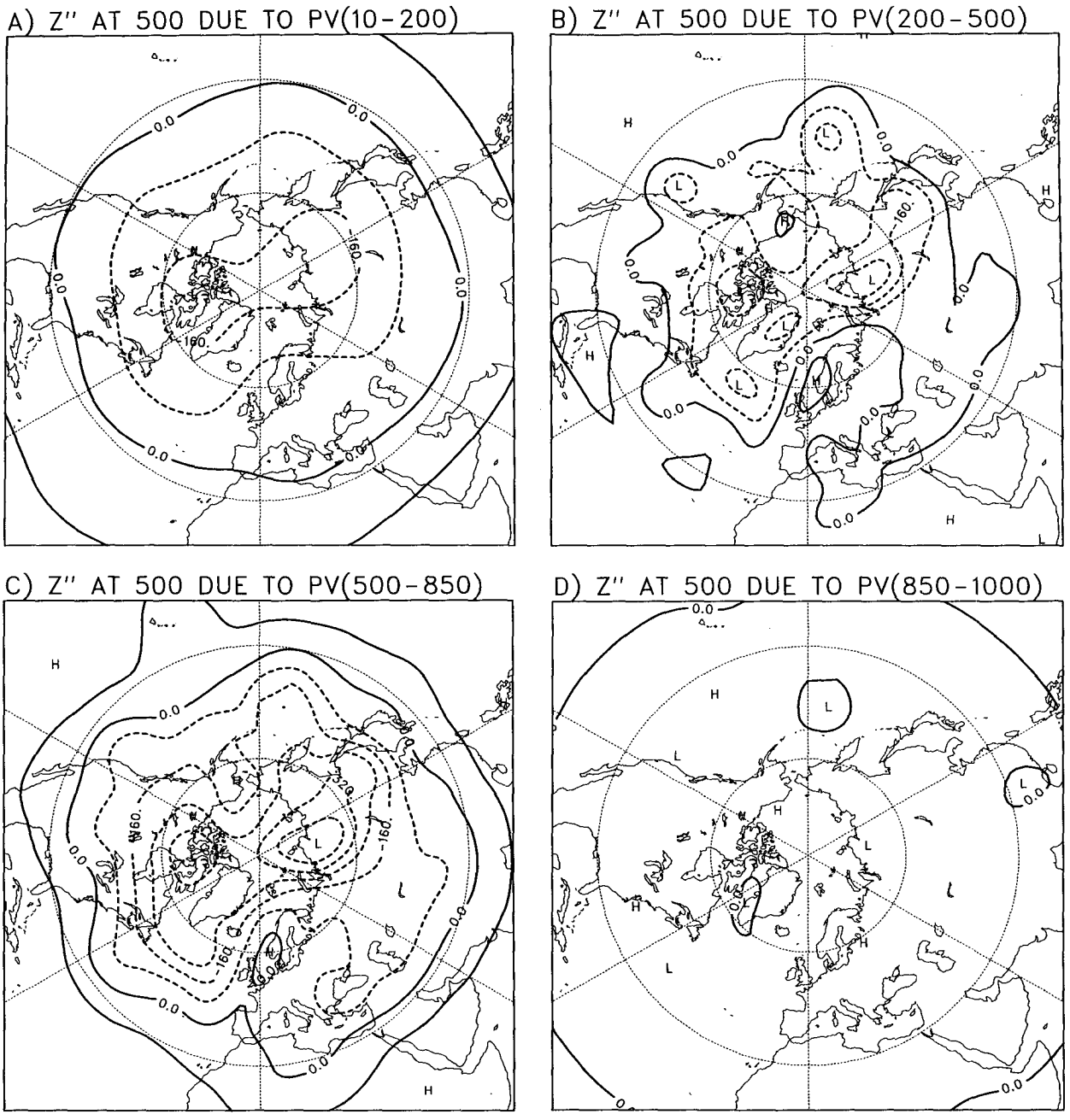

FIG. 8. Contributions to the 500 mb Z'' field at 0000 UTC 21 February 1979 arising from the PV in the layers indicated. The sum of the four fields is that seen in Fig. 3b. Isoline spacing is 80 m, negative values are indicated by dashed lines.

A possibly useful way of decomposing the flow might be to look at the contribution of individual layers to three-dimensional flow by essentially treating the boundary temperatures of a layer as thin sheets of PV. The results obtained in this way indicate, in contrast to traditional thinking, that low-level PV anomalies have little effect on the upper-level flow but that upper-level PV anomalies have a major impact on the large-scale flow at the lower levels.

This method could be useful in the validation of numerical weather prediction models. For example, one could study specific events, such as strong cyclogenesis or blocking, and see how the loss of predictability by a given model arises due to a poor prediction of PV in various layers.

Acknowledgments. The help of Carl Fortelius in some data processing problems and comments by Kimmo Ruosteenoja and three official reviewers on the manuscript are acknowledged.

APPENDIX

Numerical Algorithm Used in Partitioning the Flow

The atmosphere between 10 and 1000 mb was divided into 99 equal layers so that the grid interval (Δp) in the vertical was 10 mb. Observed quantities (C, B, and σ_{ref}) were interpolated into this grid using cubic splines. Derivatives were then replaced by centered differences, whereafter (13) could be written for each wave component n, m in the form:

$$\mathbf{AX} = \mathbf{D}, \tag{A1}$$

where the band matrix $\mathbf{A}$ depends on σ_{ref} and the wavenumber. The vector $\mathbf{X}$ includes the unknown variable χ and the vector $\mathbf{D}$ includes the forcing C and the boundary temperature B.

When the total reconstructed field was calculated, the complete form of $\mathbf{D}$ was used:

$$\mathbf{D} = \begin{pmatrix} B_T & + & 0 \\ \vdots & & \\ (x_{h+4} - x_{h+2})/2\Delta p & + & y_{h+3} \\ (x_{h+3} - x_{h+1})/2\Delta p & + & y_{h+2} \\ (x_{h+2} - x_{h})/2\Delta p & + & y_{h+1} \\ (x_{h+1} - x_{h-1})/2\Delta p & + & y_{h} \\ (x_{h} - x_{h-2})/2\Delta p & + & y_{h-1} \\ (x_{h-1} - x_{h-3})/2\Delta p & + & y_{h-2} \\ (x_{h-2} - x_{h-4})/2\Delta p & + & y_{h-3} \\ \vdots & & \\ B_L & + & 0 \end{pmatrix} \tag{A2}$$

where x is the spherical harmonic coefficient of

$$\frac{f_o \theta''}{d\theta_{\text{ref}}/dp}$$

and y is the corresponding coefficient of

$$\frac{1}{f_o} \nabla_p{}^2 \Phi''.$$

Here B_T and B_L are the corresponding coefficients arising from the contribution of the boundary temperature at the top and bottom of the atmosphere.

The decomposition of the flow into components arising from the interior PV and the boundary temperature, as well as from the VORT and STAB part, was obtained by retaining/deleting corresponding terms in (A2). When the flow was partitioned by using (7), x and y were set equal to zero outside the layer k; B_T or B_L was included only if the layer considered was adjacent to the 10-mb level or 1000-mb level, respectively. For example, if the layer was confined by levels $h - 1$ and $h + 1$, its contribution was calculated by having

$$\mathbf{D} = \begin{pmatrix} 0 & + & 0 \\ \vdots & & \\ 0 & + & 0 \\ -x_{h+1}/2\Delta p & + & 0 \\ -x_{h}/2\Delta p & + & y_{h+1} \\ (x_{h+1} - x_{h-1})/2\Delta p & + & y_{h} \\ x_{h}/2\Delta p & + & y_{h-1} \\ x_{h-1}/2\Delta p & + & 0 \\ 0 & + & 0 \\ \vdots & & \\ 0 & + & 0 \end{pmatrix}.$$

In this manner the atmosphere could be divided into layers, the sum contribution of which gives exactly the total reconstructed geopotential field. Note that in this numerical representation, the PV sheets, discussed in section 5, at the upper and lower boundary of the layer considered are represented by derivatives of large magnitude at both boundaries.

REFERENCES

Bretherton, F. P., 1966: Critical layer instability in baroclinic flows. *Quart. J. Roy. Meteor. Soc.*, **92**, 325–334.

Egger, J., 1990: Some aspects of potential vorticity inversion. *J. Atmos. Sci.*, **47**, 1269–1275.

Green, J. S. A., 1987: Comments on "On the use and significance of isentropic potential vorticity maps." *Quart. J. Roy. Meteor. Soc.*, **113**, 401–402.

Holopainen, E. O., 1970: An observational study of the energy balance of the stationary disturbances in the atmosphere. *Quart. J. Roy. Meteor. Soc.*, **96**, 626–644.

Hoskins, B. J., 1983: Modelling of the transient eddies and their feedback on the mean flow. *Large-scale Dynamical Processes in the Atmosphere*, B. J. Hoskins and R. P. Pearce, eds., Academic Press, 169–199.

——, M. E. McIntyre, and A. W. Robertson, 1985: On the use and significance of isentropic potential vorticity maps. *Quart. J. Roy. Meteor. Soc.*, **111**, 877–946.

——, ——, and ——, 1987: Reply to Green (1987). *Quart. J. Roy. Meteor. Soc.*, **113**, 402–404.

Lau, N-C., and E. O. Holopainen, 1984: Transient eddy forcing of the time-mean flow as identified by geopotential tendencies. *J. Atmos. Sci.*, **41**, 313–328.

McIntyre, M. E., and W. A. Norton, 1990: Dissipative wave-mean interactions and the transport of vorticity or potential vorticity. *J. Fluid Mech.*, **212**, 403–435.

Pfeffer, R. L., 1987: Comparison of conventional and transformed Eulerian diagnostics in the troposphere. *Quart. J. Roy. Meteor. Soc.*, **113**, 237–254.

Robinson, W. A., 1988: Analysis of LIMS data by potential vorticity inversion. *J. Atmos. Sci.*, **45**, 2319–2342.

Smagorinsky, J., 1963: General circulation experiments with the primitive equations. I: The basic experiment. *Mon. Wea. Rev.*, **91**, 99–164.

Tanaka, H., 1985: Global energetics analysis by expansion into three-dimensional normal mode functions during the FGGE winter. *J. Meteor. Soc. Japan*, **63**, 180–200.

Wiin-Nielsen, A., 1962: On transformation of kinetic energy between the vertical shear flow and the vertical mean flow in the atmosphere. *Mon. Wea. Rev.*, **90**, 311–323.